



Pergamon

Available online at [www.sciencedirect.com](http://www.sciencedirect.com)

SCIENCE @ DIRECT®



[www.actamat-journals.com](http://www.actamat-journals.com)

Acta Materialia 51 (2003) 387–405

# Deformation of electrodeposited nanocrystalline nickel

K.S. Kumar <sup>a,\*</sup>, S. Suresh <sup>a</sup>, M.F. Chisholm <sup>b</sup>, J.A. Horton <sup>b</sup>, P. Wang <sup>c</sup>

<sup>a</sup> Department of Materials Science and Engineering, Massachusetts Institute of Technology, Cambridge, MA 02139, USA

<sup>b</sup> Solid State Division and Metals and Ceramics Division, Oak Ridge National Laboratory, Oak Ridge, TN 37831, USA

<sup>c</sup> Division of Engineering, Brown University, Providence, RI 02912, USA

Received 16 July 2002; accepted 20 August 2002

## Abstract

The mechanisms of deformation and damage evolution in electrodeposited, fully dense, nanocrystalline Ni with an average grain size of ~30 nm and a narrow grain size distribution were investigated by recourse to (i) tensile tests performed in situ in the transmission electron microscope and (ii) microscopic observations made at high resolution following ex situ deformation induced by compression, rolling and nanoindentation. Particular attention was also devoted to the characterization of the structure in grain interiors and in the vicinity of grain boundaries at Angstrom-level resolution in the as-deposited material and following compression, and to the real-time video-imaging of the evolution of dislocation activity and damage during deformation; these images are presented in this paper and in the web sites provided as supplementary material to this paper. These observations clearly reveal that dislocation-mediated plasticity plays a dominant role in the deformation of nanocrystalline Ni examined in this study. Fracture surface examination confirms dimpled rupture with the scale of the dimples being several times larger than the grain size. Dislocation emission at grain boundaries together with intragranular slip and unaccommodated grain boundary sliding facilitate the nucleation of voids at boundaries and triple junctions. Individual monocrystal ligaments, formed by the growth/linking of these voids, undergo extensive local plasticity to the extent that many of them neck down to a chisel point. These voids as well as those that may have existed prior to deformation can act as nucleation sites for dimples leading to fracture that does not occur preferentially along grain boundaries. The transmission electron microscopy observations of in situ and ex situ deformed specimens are synthesized to formulate a mechanistic framework that provides new insights into the mechanisms of flow and fracture in nanostructured metals.

© 2002 Acta Materialia Inc. Published by Elsevier Science Ltd. All rights reserved.

**Keywords:** Nanocrystalline metal; Deformation; Fine structure; In situ microscopy; Dimpled rupture

## 1. Introduction

Nanocrystalline metals exhibit ultra-high yield and fracture strengths, superior wear resistance,

and enhanced superplastic formability at lower temperatures and faster strain rates compared to their microcrystalline counterparts [1–6]. These attributes have generated considerable interest in the use of these metallic systems with nanometer scale grains for a wide variety of structural and functional applications (see, for example, proceedings of the international conferences, Nano2000

\* Corresponding author. Permanent address: Division of Engineering, Box D, Brown University, Providence, RI 02912, USA.  
E-mail address: [sharvan\\_kumar@brown.edu](mailto:sharvan_kumar@brown.edu) (K.S. Kumar).

and Nano2002, held in Sendai, Japan, in 2000 and Orlando, Florida, in 2002, respectively.). Several laboratory-scale processing techniques are currently available to produce such materials. They include gas-phase condensation of particulates and consolidation [7], mechanical alloying and compaction [8], severe plastic deformation [9] and electrodeposition [10–12].

A survey of literature (see next section) readily reveals that careful experimental documentation of mechanisms underlying deformation and damage evolution in nanocrystalline metals of high purity and full density with a narrow range of grain size in the nm range is presently limited, despite the large number of investigations devoted to the examination of their mechanical response. In this paper, we report transmission electron microscopy observations of the mechanisms associated with *ex situ* and *in situ* deformation in electrodeposited nickel, whose as-deposited structure was confirmed to be fully dense, with an average grain size of ~30 nm, a narrow grain size distribution, a columnar grain shape with an aspect ratio of 3 to 10, low starting dislocation density, and grain boundaries devoid of second phase particles. We document concurrent mechanisms involving void formation at grain boundary triple junctions, grain boundary separation, and transgranular plastic flow by dislocation motion and possibly twinning during deformation. These phenomena are used to provide a rationale for ductile failure processes observed on the fracture surfaces, where dimples span several grain diameters. Together, these observations are synthesized to develop insights into the mechanisms of plastic flow and ductile failure in nanocrystalline metals.

## 2. Background and literature survey

The mechanical properties of fcc metals (Cu, Ni and Pd) with grain sizes less than 100 nm, primarily extracted from experiments involving uniaxial tension and microindentation loading, have been reported [12–17]. In most cases, the material has been produced either by gas phase condensation followed by consolidation, or by electrodeposition. In the former processing route, incomplete

densification is known to influence the mechanical properties. In the latter, possible roles of texture, pre-existing voids, columnar grain structure, and hydrogen, carbon and sulfur either in solid solution or segregated to grain boundaries in influencing mechanical response are only beginning to be carefully documented [18]. Typically, the nanocrystalline metals exhibit significantly higher yield strength, and reduced tensile elongation relative to their microcrystalline counterparts. Furthermore, hardness and yield strength have been found to increase with decreasing grain size in this regime down to at least 20 nm. The reasons for this behavior are still under debate as dislocation sources within grains are not expected to operate at these grain sizes. In addition, there is no documented evidence of dislocation pile-ups in deformed specimens, and any dislocation activity is primarily believed to originate and terminate at grain boundaries. Furthermore, there is some experimental evidence indicating [19,20] that below a certain grain size (~20 nm), strength decreases with further grain refinement (the so-called “inverse Hall-Petch-type” relationship) and in this regime, grain boundary sliding and/or Coble creep apparently constitute the dominant deformation modes; yet, there appears to be no direct experimental confirmation in the published literature of the operation of these processes.

In contrast, there have been numerous computational simulations of the deformation of nanocrystalline metals (particularly Ni and Cu) [21–28] and these have typically encompassed grain sizes smaller than 15 nm except for two recent reports: the first [27] where columnar grains of Al were simulated in the grain size range 20–70 nm, and the other [28] where equiaxed grains with a grain size of 20 nm were examined. These studies collectively show that as the grain size decreases, dislocation activity ceases and grain boundary sliding dominates below grain sizes of typically 10 nm. However, there are several mechanisms postulated from these simulations that lack experimental backing. Thus, in the 15–70 nm grain size regime in Al, at a sufficiently high stress, a leading Shockley partial is postulated to be emitted from a grain boundary or triple junction and if the grain size is sufficiently large compared to the splitting distance

between the leading and lagging partial, a second partial would also emit with the extended dislocation traversing the grain. If the grain size is small relative to the splitting distance, the leading partial would find its way to the adjacent boundary leaving a faulted grain behind [27]. In the grain size regime between roughly 10–15 nm, grain boundary sliding and dislocation glide are predicted [25] whereas at a grain size of ~5 nm, no dislocation activity is observed in the computational simulation. Furthermore, a mechanism is proposed by which partial dislocations are emitted from the grain boundaries into the grains [28]. It is pertinent to recognize that all these simulations entail atomistic computations and therefore only capture the very early stages of deformation. Furthermore, these simulations do not make allowance for damage evolution and fracture and therefore, instantaneous loading, in a matter of picoseconds, to very high stress levels in unrealistically high, dynamic strain rate regimes in the computational simulations preclude creep mechanisms and could trigger deformation modes which may not typically be activated in experiments.

The deformed microstructure in nanocrystalline metals has been examined in the electron microscope for evidence of dislocation activity, but the resultant dislocation debris characteristic of deformed metals has not been observed [14]. Such observations, together with the results of the simulations, have led to the general notion that grain boundary sliding is the dominant deformation mechanism in these materials, particularly at grain sizes less than 20 nm.

A few in situ deformation studies have also been conducted in the transmission electron microscope (TEM) [29–31] with the objective of observing dislocation motion, or grain boundary sliding and grain rotation activity as they occurred. The first of these studies was performed on 8 nm and 25 nm gold that had been sputtered onto an electron-transparent Al substrate. The still images in this paper [29] show some evidence of plastically deformed ligaments bridging secondary cracks as well as the presence of what the authors refer to as “nanopores” at grain boundaries. Crack growth along grain boundaries is claimed and no direct evidence of dislocation activity in the 8 nm grain

size film is documented. In addition, linear defects which “may be dislocations or twins” were ostensibly observed in the 25 nm grain size film, although no images of such defects were presented in the paper. Their high-resolution image was taken after fracture and thus, although the specimen was loaded to failure within the microscope, the image documentation process was effectively the same as that for an ex situ specimen. Absence of dislocations in such an image does not confirm that dislocation activity did not exist during deformation.

In order to investigate the existence of dislocation activity during deformation, it is essential to record the deformation process as it occurs, by recourse to a videocamera or an equivalent instrument. This was recently accomplished by Youngdahl et al. [30] using nanocrystalline copper specimens produced by inert gas condensation followed by compaction. The material was reported as being 97% dense and having a broad grain size distribution range from 20–500 nm although “the majority” was between 50–80 nm. These authors reported plastic deformation being prominent ahead of the crack tip and less evident in its wake. In grains as small as 50 nm, it is claimed that parallel arrays of mobile dislocations were observed, although no images were provided. In addition, down to a grain size of 30 nm, they observed no evidence for dislocation pile-ups at grain boundaries, or grain boundary sliding or grain rotation. Furthermore, it was noted that transgranular deformation activity in grains smaller than 30 nm in size could not be visualized due to problems related to “overlapping grains”.

McFadden et al. [31] reported observations of an in-situ deformation study of nanocrystalline IC-218, a complex Ni-based superalloy containing 0.15 at.% boron. The nanocrystalline structure was obtained through severe plastic deformation, and although they explicitly do not provide an average grain size or a grain size distribution in the paper, the TEM in-situ images suggest grain sizes that are of the order of 100–150 nm. These authors state that little dislocation activity occurred in the grains, and that grain boundary sliding and grain rotation were observed, although no evidence was provided. This is somewhat surprising considering the grain size regime although the structure and

dislocation content of grain boundaries in materials produced by severe plastic deformation are not well understood at present; furthermore, the role of boron which typically segregates to grain boundaries in Ni<sub>3</sub>Al in facilitating sliding at boundaries cannot be ignored. The majority phase in this multiphase alloy is Ni<sub>3</sub>Al, an ordered compound with the L1<sub>2</sub> structure in which superdislocations with an  $a < 110 >$  Burgers vector dissociated into two superpartials separated by an antiphase boundary (APB) domain are known to operate. Furthermore, the APB energy is anisotropic in this compound, being the lowest in the cube planes. This promotes cross slip of the screw segments onto the cube plane where they are sessile. Thus, dislocation motion in this compound is complex and has been the subject of considerable debate over the past 30 years [32]. The inability to nucleate and move dislocations in the grain size regime discussed in [31] could be a consequence of the structure and chemistry of the ordered alloy, and might not be attributable to the sole influence of grain size on deformation.

It is evident from the foregoing discussion that very limited fundamental understanding exists of the deformation and damage evolution in nanocrystalline metals. The present study was, therefore, initiated with the specific objective of observing, both during and after deformation, the mechanisms of deformation and damage using state-of-the-art experimental tools in, fully dense nanocrystalline Ni with a narrow range of grain sizes.

### 3. Material and experimental procedure

The material chosen for experimental investigation was electrodeposited nanocrystalline (nc) Ni. Among various possibilities available for the production of nanostructured metals and alloys, the electrodeposition route was deemed attractive for the present investigation because this method is capable of producing relatively larger quantities (for example, 25 cm × 25 cm × 0.1–0.2 mm thick) of a fully-dense metal (and some simple binary alloys) in a single batch with an average grain size < 50 nm and a fairly narrow grain size distribution. This permits meaningful evaluation of

mechanical properties from a single material source wherein the structure is essentially free of processing-induced defects. The grain structure in electrodeposited nanocrystalline materials can vary from columnar to equiaxed depending on the processing conditions. Impurities in the material are typically limited to interstitial types, particularly hydrogen, which can exist in solid solution or precipitate in the form of bubbles within the grains and at grain boundaries and triple junctions. Nucleation aids are often added to the electrodeposition bath to produce the nanocrystalline structure and their effects on measured properties are not fully understood. The use of additives such as coumarin and saccharin can introduce carbonaceous material or sulfur into nickel, and these can lead to solid solution strengthening and grain boundary embrittlement. The interactions between bath pH, grain size, co-deposition of hydrogen and crystallographic texture in the deposit are described by Ebrahimi et al. [13].

The material used in the present experimental studies was procured from two different sources. The first source [4] entailed preparation of the material in a NiSO<sub>4</sub>·6H<sub>2</sub>O (300 g/L)+NiCl<sub>2</sub>·6H<sub>2</sub>O (45g/L)+boric acid (45g/L) bath containing saccharin (5g/L) and sodium lauryl sulfonate (0.25g/L). The bath was maintained at a pH level of 2.0 and at 65 °C; a current density of 0.05 A/cm<sup>2</sup> was used and plating was carried out for 30 min. The resulting deposit was in the form of a sheet with thickness varying between 20 and 30 μm. The surface roughness of the sheet was characterized using a conventional scanning electron microscope (SEM). Detailed atomic-resolution observations of the grain structure in the as-deposited condition and TEM bright field observations following cold-rolling of this material were made using the procedures outlined in the following sections. The second source of electrodeposited Ni resulted in sheets that were approximately 100 μm in thickness with an average grain size of ~40 nm [33,34]. This material was used to study the mechanisms of deformation and damage induced by uniaxial compression and nanoindentation, as well as for the in-situ tensile tests conducted in the TEM.

Thin foil specimens, 3 mm in diameter, for observation in the TEM were prepared by the con-

ventional twin-jet polishing technique using a nitric acid-methanol solution (25% by volume of  $\text{HNO}_3$ ) at  $-40\text{ }^\circ\text{C}$  and 7 V. The general microstructure was examined in the bright field mode in a Phillips 420 TEM operating at 120 kV whereas the ultra-fine structure was examined using a Vacuum Generators HB603U scanning transmission electron microscope (STEM) operating at 300 kV.

Disks of the material, 3 mm in diameter, were deformed *ex situ* by uniaxial compression, by rolling between two stainless steel sheets, and by nanoindentation, and subsequently examined in the TEM for evidence of dislocation activity. The uniaxial compression test was conducted by stacking several of the 3-mm disks on top of one another to achieve a sample of reasonable height (each disk was  $\sim 100\text{ }\mu\text{m}$  in thickness). The thickness of an individual disk after the test was measured to obtain an estimate of the plastic strain ( $\sim 4\%$ ). This disk was then electropolished and examined in the TEM. In contrast, the rolled specimen (repeated passes with an incremental decrease in the roll gap) experienced a height decrease of  $\sim 15\text{--}20\%$ .

The 3-mm diameter disk for nanoindentation was first mechanically ground and finish-polished on both sides to obtain a surface suitable for nanoindentation. The specimen was then placed on a VCR dimpler stage (model number; D500i, South Bay Technology, San Clemente, CA) and dimpled on one side. Next, the specimen was transferred to a nanoindenter (NanoTest, MicroMaterials, Wrexham, UK) and approximately 100 indents were placed in a geometrical array on the flat surface, the center of the array being located off to one side of the specimen center but contained in an area of the flat surface still directly above the dimpled region. The maximum depth of indentation was 200 nm, with the corresponding maximum load being in the range 8.0–9.5 mN. Finally, the specimen was transferred to an ion-milling stage that was cooled with liquid nitrogen and was single-gun milled on the dimpled side to perforation. The resulting electron-transparent area was examined in the TEM to determine if it contained one or more of the indentations; the regions adjacent to an indentation were examined carefully to identify the presence of any dislocation debris.

Several sub-size, dog-bone-shaped tensile speci-

mens (7.0 mm long by 3.0 mm wide by approximately 0.09 mm thick) were electro-discharge-machined from the nanocrystalline Ni sheet for the purpose of *in situ* testing in the TEM. Each specimen had a pair of holes, 1.0 mm in diameter and with a center-to-center distance of 4 mm, machined into it for purposes of pin-loading. A reduced gage section was also built into each specimen. Such specimens were then twin-jet polished as described above to produce a perforation in the center of the gage section. The specimens were then incrementally strained in discrete steps in a Philips CM30 TEM operating at 300 kV to generate cracks from the perforation, with the cracks typically advancing perpendicular to the loading direction. The regions ahead of these crack-tips were then monitored to identify the dominant deformation mechanisms. The specimen was loaded by applying either continuous or pulsed displacement manually through a toggle switch that activated a motor in the TEM stage. Attempts to capture the progress of events using still photographic images were not successful because of the rapid mobility of the dislocations. The entire deformation process was, therefore, video-recorded continuously. Segments from the videotape were extracted and digitized. Sequences of still images were then extracted from such digitized clips, some examples of which are included here. The fracture surfaces of the broken specimens were examined in a Hitachi S4100 scanning electron microscope (SEM) to document the dominant fracture mode.

## 4. Results

### 4.1. As-deposited microstructure

An SEM examination of the surface of the electrodeposited nc-Ni sheet away from the substrate confirmed a rough nodular morphology that is a consequence of deposition and care must be exercised to smoothen the surface by grinding to eliminate these features prior to mechanical testing. Such surface roughness has been previously observed and discussed [33]. General bright field TEM images of the structures of the as-received nc-Ni sheets are shown in Figs. 1a–c. The plan

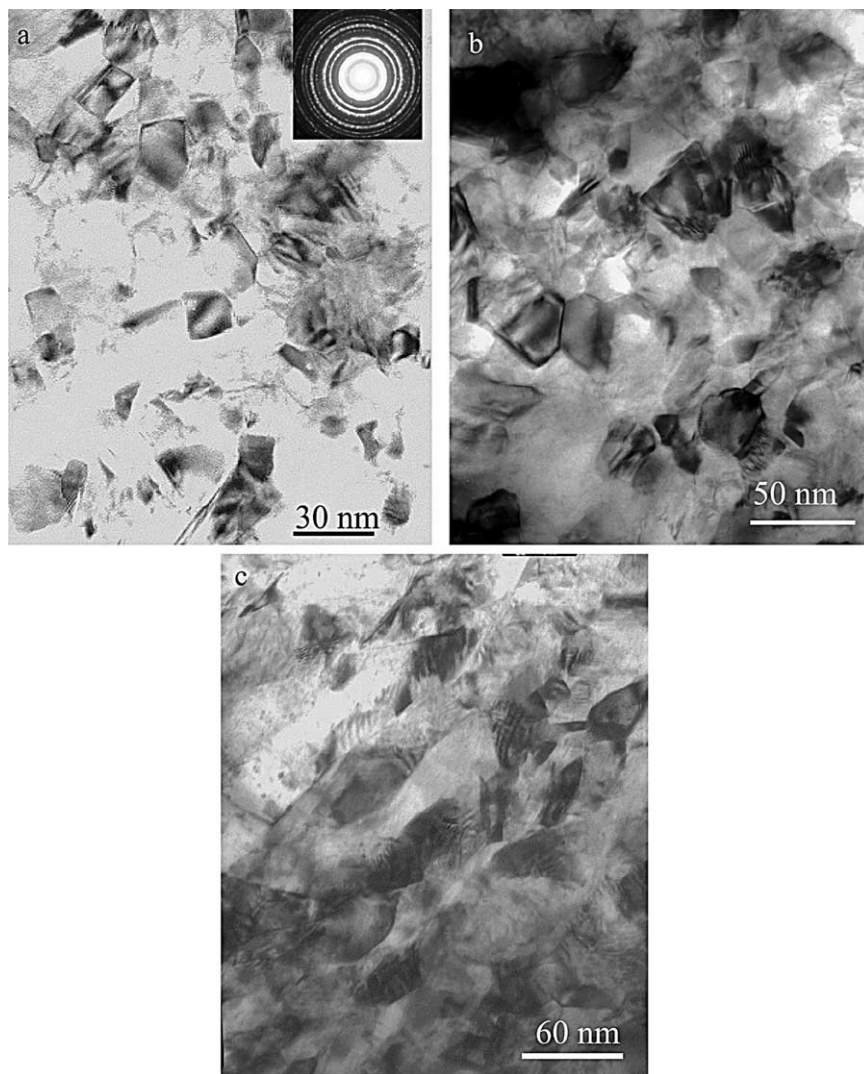


Fig. 1. Bright Field TEM images showing (a,b) the plan view of the as-deposited structure of nc-Ni from (a) source 1 [4], and (b) source 2 [33,34]. In (c), the cross-section view of the nc-Ni sheet from source 2 confirms a columnar grain structure.

views (Figs. 1a,b) confirm a fairly narrow grain size distribution with a mean grain size of approximately 30 nm for the electrodeposited Ni procured from the first source [4] and approximately 40 nm for the material from the second source [33,34]. In both materials growth twins are prevalent. The grain interior appears to be clean and devoid of dislocations. The grain boundaries show no evidence of second phase particles or films. A selected area diffraction pattern shown as an inset in Fig. 1a confirms the expected ring pattern for such

ultra-fine-grained materials and analysis of the pattern verified a single-phase, face centered cubic Ni structure. Cross-sectional TEM images of the material from the second source [33,34] verified that the grains have a significant aspect ratio (columnar structure) but the column lengths are insignificant compared to the sheet thickness (Fig. 1c).

High-resolution images obtained using the VG-STEM are shown in Figs. 2-5 for the two materials. An examination of the grain interior using a pair

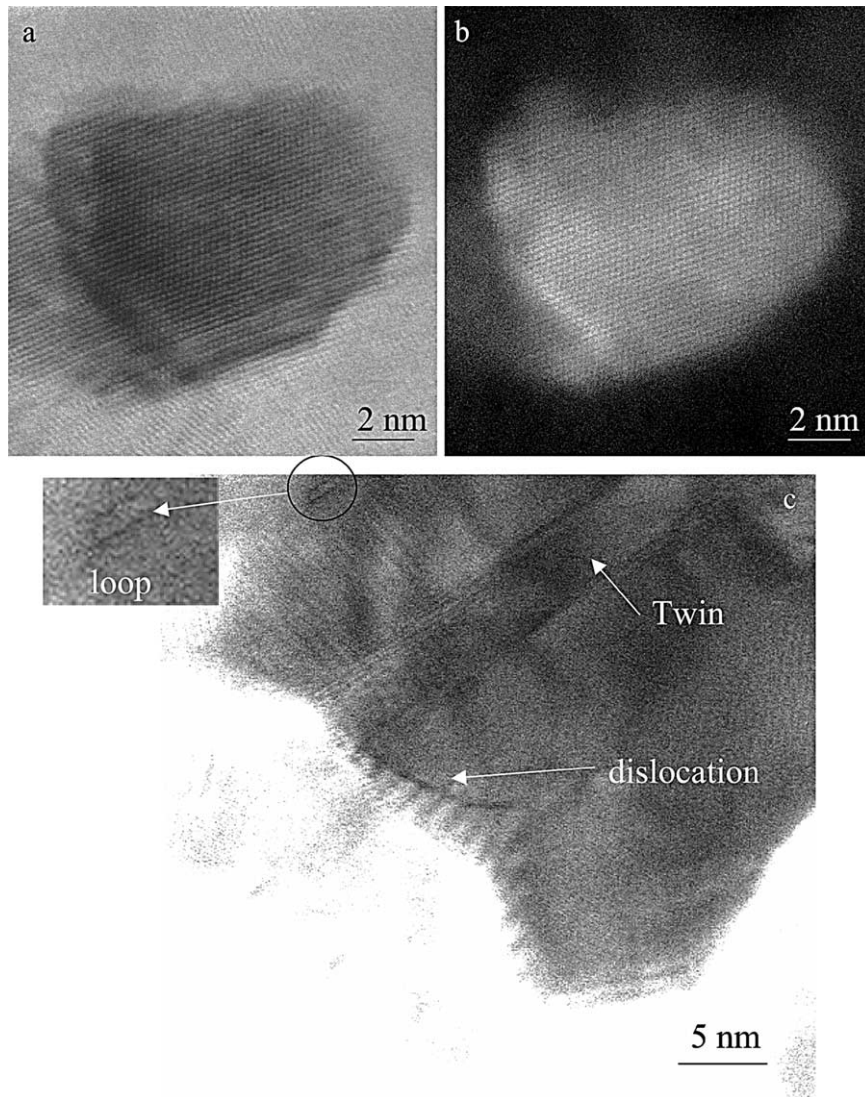


Fig. 2. High resolution STEM images of the nc-Ni from source 1 [4]: (a, b) bright field-dark field pair confirming a crystalline structure in the grain interior that extends all the way to the grain boundary with no indication of dislocations within the grains, and (c) another grain that contains a twin, a single dislocation at the boundary and a small dislocation loop within the grain.

of bright field-dark field images (Figs. 2a,b) confirms a structure which is devoid of dislocations and which maintains a well-ordered crystal structure right up to the boundary. An annealing twin, an isolated curved dislocation line, and a nanometer-sized dislocation loop are observed in another grain (Fig. 2c). These images and other similar ones confirm the low initial dislocation content in the individual grains in the as-deposited

material. Fig. 3a confirms the absence of any grain boundary phase or amorphous regions at a multiple grain junction in this material. A grain boundary, which is imaged edge on in Fig. 3b, unambiguously demonstrates that crystallinity is maintained up to the grain boundary and that the boundary is micro-faceted on the {111} planes. These findings are in agreement with earlier experimental reports on the fine structure of nanocrystalline Pd [35,36]

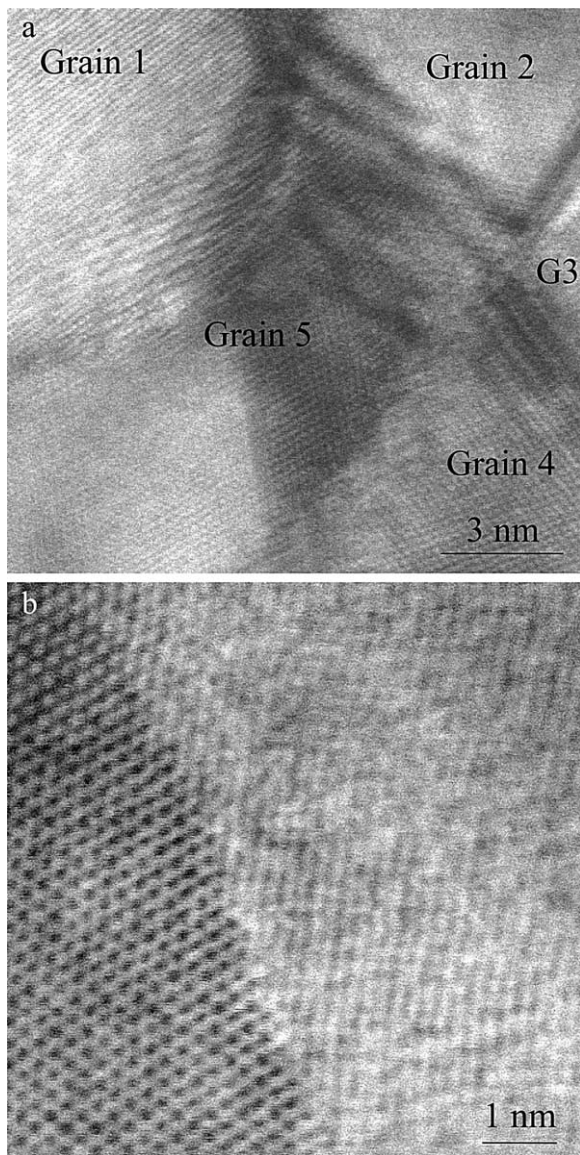


Fig. 3. High resolution STEM images of the nc-Ni from source 1 [4] showing (a) multiple grain junctions that reveal no evidence of second phase at the boundary (G3=grain 3), and (b) a clean atomically-faceted grain boundary.

and the computations of Van Swygenhoven et al. [37], but they contradict claims of the existence of an “extended grain boundary region” in such materials [38,39]. Fig. 4 shows an example of the occasional presence of periodic dislocation arrays constituting low-angle boundaries in the elec-

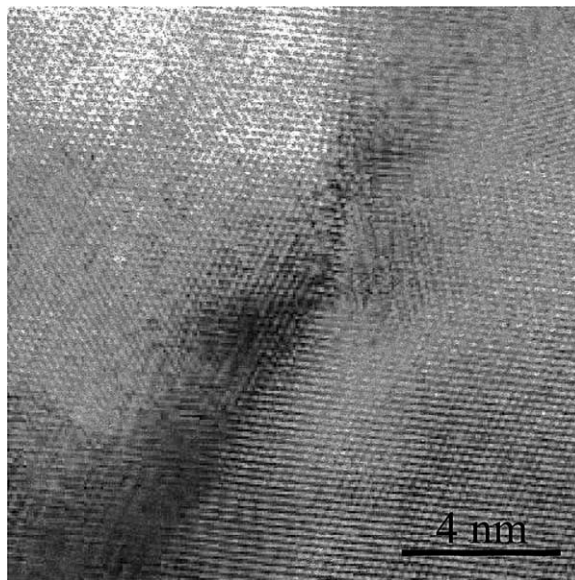


Fig. 4. High resolution STEM image of the nc-Ni from source 2 [33,34] showing the occasional presence of low-angle boundaries.

trodeposited Ni from the second source [33,34] whereas such boundaries were not readily observed in the material from the first source [4]. In all of these observations, we did not see any evidence for the presence of nanovoids either in the grain interior or at grain boundaries in these materials.

#### 4.2. Ex situ deformation

The specimen that was deformed in uniaxial compression was examined using conventional TEM and VG-STEM. Representative images in Figs. 5a–d show some evidence of dislocation debris within the grains (Fig. 5a), the possible presence of a triple junction wedge crack (Fig. 5b), a dislocation array in Fig. 5c considered to be a grown-in low-angle boundary, and a high-resolution image of a grain boundary region in Fig. 5d which again confirms that crystallinity is preserved all the way up to the boundary.

The microstructure in the vicinity of a nanoindentation in a specimen of nanocrystalline Ni is shown in Fig. 6. The triangular hole represents the indentation and the areas near the three corners and the sides of the triangle were examined at a higher

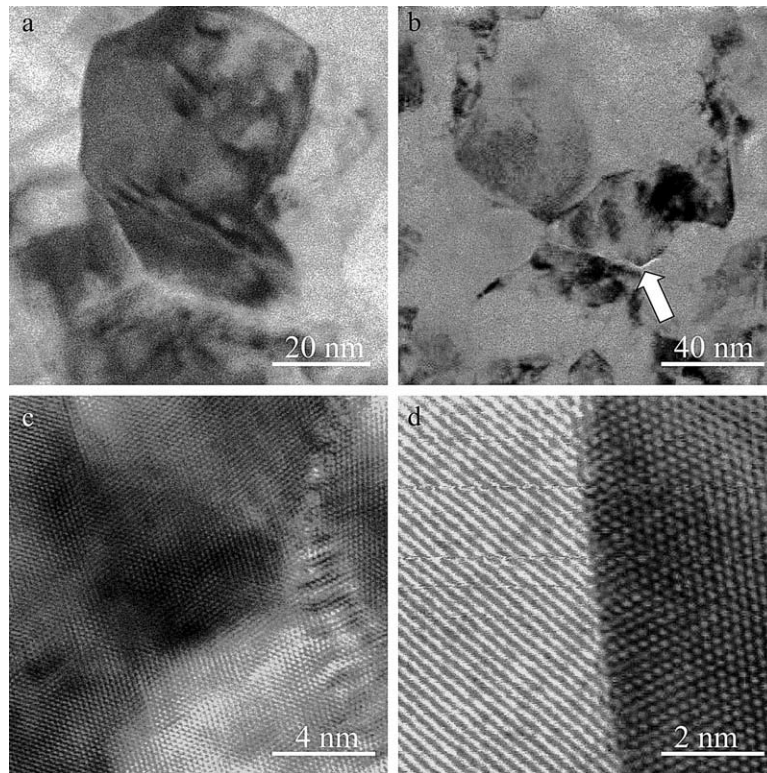


Fig. 5. Microstructure following 4% plastic strain in compression (nc-Ni from source 2): (a) bright field image showing a few dislocations within a grain, (b) a possible crack at a triple junction, (c) substantially dislocation-free grains and possibly a low-angle boundary, and (d) clean grain boundaries with no evidence of residual dislocation debris from the deformation.

magnification for evidence of dislocation activity. The occasional presence of a few isolated dislocations within some grains (an example of one such grain is indicated by an arrow in Fig. 6) cannot account for the large plastic strains accommodated by the material.

The specimen that had been cold-rolled between two stainless steel sheets was also examined by bright-field imaging in a TEM and a representative micrograph is shown in Fig. 7. The interesting features to note are that the grains appear coarser than in the as-received material and often, the grain corners at triple junctions are rounded. In addition, semi-circular strain contrast is observed at various locations adjacent to grain boundaries, reminiscent of dislocation emission (indicated by upward pointing arrows in the figure). In another grain in this figure, a pair of slip traces indicative of dislocation activity is recognized and is identified by

the downward-pointing arrows. Lastly, a feature resembling a nanovoid is noted at the triple junction. Whether this feature is a consequence of deformation is not certain, but it was the only time that it was observed. The observation of a coarser grain size than in the as-deposited state, the rounding of grain boundaries near the triple junction, and the presence of a nanovoid at the same location may all be a consequence of local diffusion due to adiabatic heating during rolling, although care was taken to keep the reduction per pass during rolling to a minimum for this reason. If this feature is a nanovoid that formed during deformation, it may have resulted either due to grain rotation or diffusional creep.

#### 4.3. *In situ* deformation

A low-magnification image of a crack generated in the thin foil by loading within the microscope

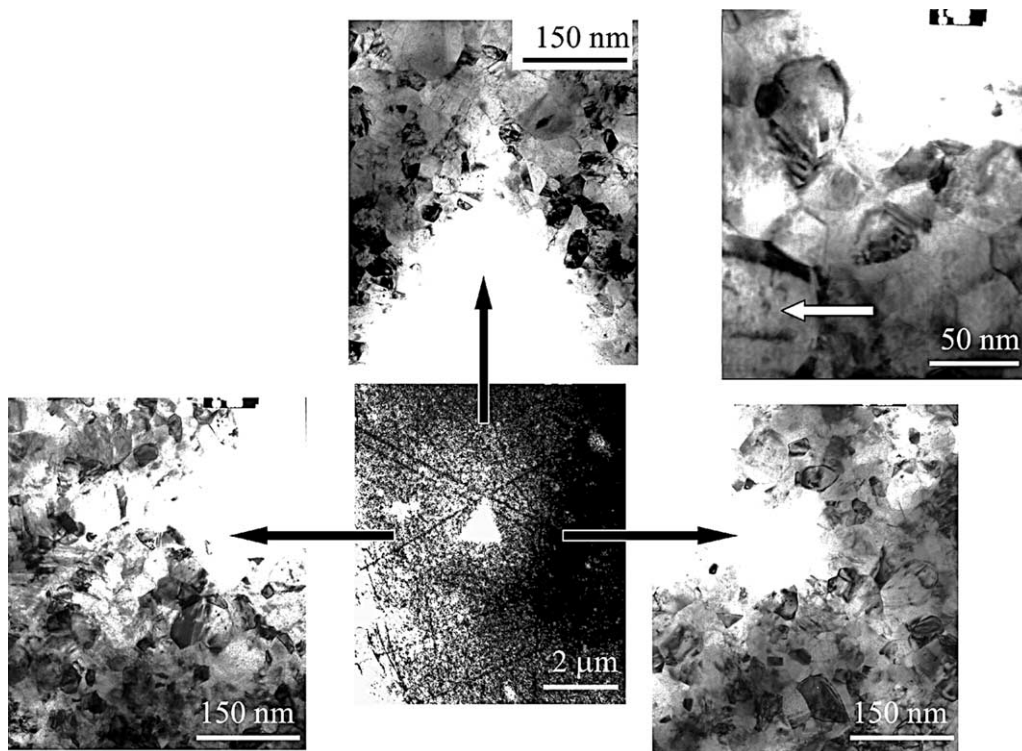


Fig. 6. Bright field images of the regions in the vicinity of a nanoindentation (nc-Ni from source 2) confirming the absence of substantial dislocation debris within the grains except in the largest of grains (see grain in top right photograph indicated by an arrow).

is shown in Fig. 8. The crack assumes a saw-tooth morphology and interestingly, several of the saw-tooth regions exhibit extensive local plastic flow where the material necks down to a point. There is, however, no direct evidence for the presence of dislocations in this image. Attempts to load the specimen so as to allow the crack to advance or blunt, to refocus the region and then to photograph it to obtain images of dislocation debris were not successful although there appeared to be significant dislocation activity immediately after loading the specimen, particularly in the vicinity of the crack tip. It became evident that the progress of deformation needed to be documented in real-time and continuously to demonstrate convincingly the presence of dislocation activity during plastic deformation. Thus the image on the screen was diverted to a video camera connected to a viewing monitor as well as to a computer capable of capturing “freeze-frame” images at various stages of the

deformation process. A sequence of such freeze-frame images is shown in Fig. 9.

In the first of this sequence of images, three grains (whose boundaries are identified by the three white arrows) and the crack tip denoted as A are seen (Fig. 9a). This image was obtained with the specimen under load after one displacement pulse. It is relevant to note that prior to applying this displacement pulse, the specimen was already under load which produced the crack arriving at this location. The white arrows in Fig. 9a illustrate the presence of grain boundary microcracks and triple junction voids. Whether these defects were produced by prior loading or they were pre-existing is not known. After four displacement pulses (Fig. 9b), the crack appears to proceed part way through grain 1 and the grain boundary cracks and triple junction void appear to have grown. A second crack (crack B) arrives in this region from the top right corner in Fig. 9b. At this stage, there

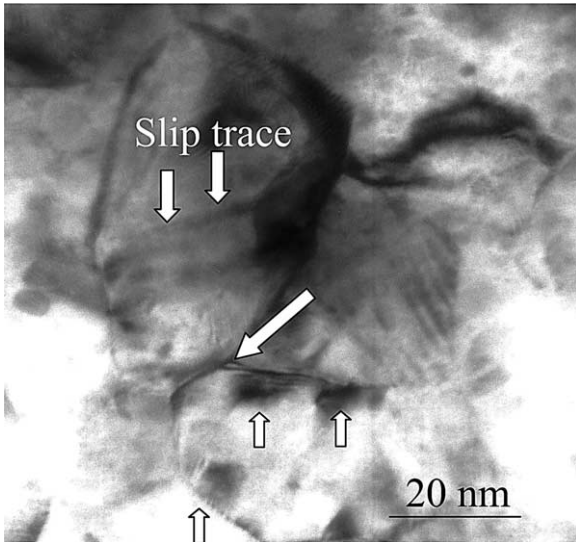


Fig. 7. A bright field TEM image of the microstructure following cold-rolling of nc-Ni from source 1 showing slip traces indicated by downward -pointing arrows, a triple junction nano-void, and semicircular strain contrast at grain boundaries indicated by upward-pointing arrows that suggest dislocation emission.

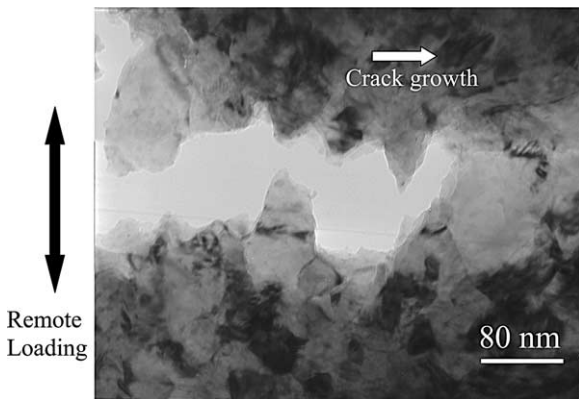


Fig. 8. A low-magnification bright field image of an advancing crack and the region around the crack tip in an in situ deformation experiment on nc-Ni from source 2 [33,34]. The image shows a saw-tooth crack profile with cracks often running across grains that have necked down plastically.

appears to be no clear evidence of substantial dislocation activity. The same location after 12 pulses is shown in Fig. 9c, where the progression of Crack A through grain 1 as well as through most of grain 2 is evident. The progression of crack B, from the

top of the image down into grain 3 is also seen, with only a segment of grain 3 left intact. An array of dislocations appears to have been emitted from crack B; at a later time, Fig. 9d, the array is still observed but it has a different configuration and the inset in Fig. 9d shows the array at this stage at a higher magnification.

Sequential still images extracted from a video clip of in situ deformation in the TEM of a nanocrystalline nickel tensile specimen are shown in Figs. 10a,b. The presence of dislocation contrast is recognized in these two figures. (Three video clips from this and other similar experiments can be viewed at <http://ninas.mit.edu/Submission/SupInfo/index2.html>). A sequence of still images extracted from another video segment is shown in Figs. 11a–d. Fig. 11a confirms the presence of a ligament consisting of three grains. These grains appear elongated; whether this is a consequence of these grains being already plastically deformed and stretched or due to the original columnar morphology of the grains is not known. Following incremental loading, the boundaries between grains 1 and 2 and between grains 2 and 3 begin to separate, as identified by the arrows in Fig. 11b. Further loading leads to the formation of a single crystal ligament (Fig. 11c) which plastically deforms and necks down to a point (Fig. 11d). Deformation is accompanied by alternate parallel bands of bright and dark contrast that are inclined to the tensile axis (Fig. 11c) and provide possible evidence of twinning. The video clip from which these still images were obtained can also be viewed at <http://ninas.mit.edu/Submission/SupInfo/index2.html>. These video clips collectively confirm extensive dislocation activity within several grains ahead of the crack tip, emission and absorption of dislocations at grain boundaries, progressive specimen thinning as plastic deformation proceeds ahead of the crack tip, and the formation/growth of grain boundary cracks and triple junction voids. The grains that bridge these cracks and voids become partially unconstrained and the resulting ligaments deform plastically to a chisel point.

#### 4.4. Fracture morphology

Several of the in situ tensile specimens were manually loaded until complete physical separation

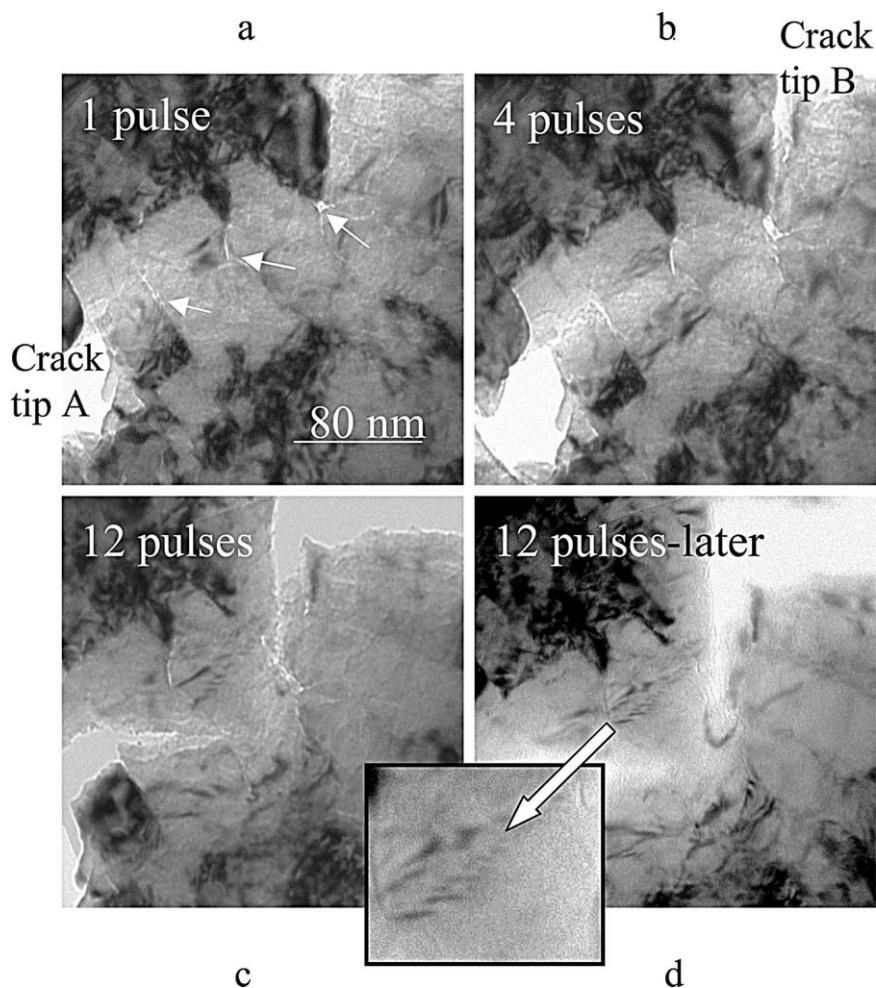


Fig. 9. A sequence of “freeze-frame” images captured during an in situ deformation test in the TEM of a microtensile specimen from source 2 [33,34]. Images a–d show the microstructural evolution and progression of damage with an increase in the applied displacement pulses. The presence of grain boundary cracks and triple-junction voids (indicated by white arrows in (a)), their growth, and dislocation emission from crack tip B in (b–d) in an attempt to relax the stress at the crack tip as a consequence of the applied displacement, can all be seen. The magnified inset in (d) highlights the dislocation activity.

occurred. The resulting cross-sections representing the fracture surfaces were examined in the SEM. A low magnification image of one half of a tensile specimen is shown in Fig. 12a. The specimen grip section with the pin hole, the electropolished region in the gage section and a portion of the perforation in the foil stemming from jet polishing can all be seen in this figure. The relatively thin segment of the specimen, within the electropolished region, demonstrates the presence of several ductile ligaments (some of which are indicated by

arrows in Fig. 12b); these ligaments undergo charging in the electron microscope and appear as bright features in the image. They can also be identified with the chisel-tip features seen during deformation, such as the one observed in Fig. 11d. The fracture surface corresponding to the thicker section of the specimen (Fig. 12c) illustrates dimpled rupture. The average size of the dimples is six to ten times the average grain size. An examination of a specific location on a pair of mating fracture surfaces confirmed the presence of these dimples

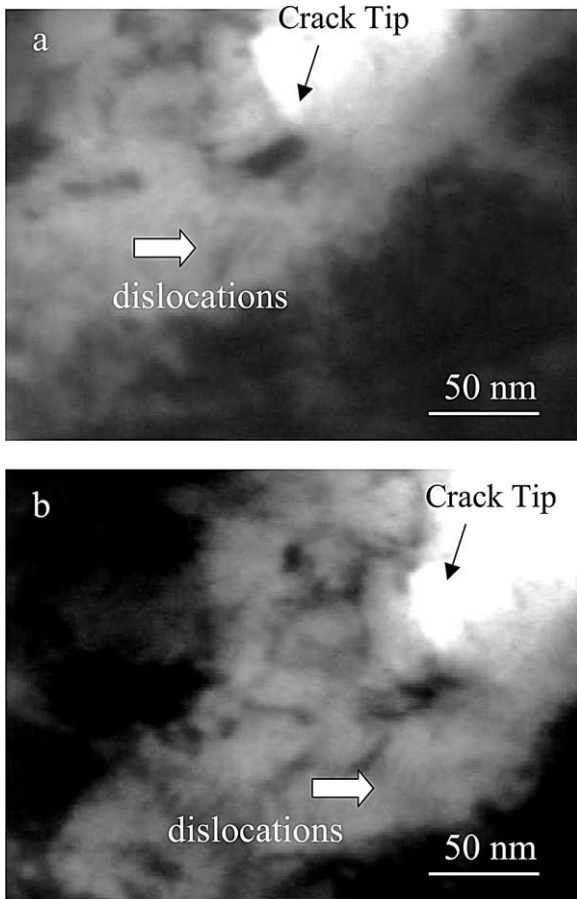


Fig. 10. A pair of images extracted from a video-tape recording of the progression of deformation in an in situ straining experiment. The video images were subsequently digitized and still frames were extracted from the digitized segment. The images show dislocation activity within the grains. The speed of image capture was 1/30 of a second between successive frames. The digitized clip may be viewed at <http://ninas.mit.edu/Submission/SupInfo/index2.html>.

on both surfaces (Figs. 13a,b). These SEM observations together with the in situ TEM results of extensive dislocation activity at crack tips demonstrate the dominant role of dislocation plasticity during deformation of nanocrystalline nickel.

The dimples observed on the fracture surface of the present in situ tensile test specimens exhibit features that are similar to those seen on the failure surfaces of electrodeposited nanocrystalline Ni subjected to ex situ quasi-static and dynamic tensile deformation [40] and e-beam deposited nanoc-

rySTALLINE Al-Fe binary solid solution alloys [41] following quasi-static as well as high-strain rate deformation.

## 5. Discussion

Available experimental and computational results illustrate that the yield strength of nanocrystalline metals and alloys increases with decreasing grain size down to at least 10–15 nm; below this grain size, the yield strength either levels off or decreases with a further decrease in grain size. For grain sizes in the micrometer range and down to at least 100 nm, the increase in strength with decreasing grain size is usually attributed to the well-known Hall-Petch relationship, although there appears to be no well-accepted model (based on dislocation processes) that explains this strengthening mode unambiguously. The mechanisms responsible for the observed behavior below a grain size of ~100 nm are still not well established. There is, however, general consensus that plastic deformation mediated by dislocation activity is still likely the primary deformation mode at least down to 30 nm. At grain sizes of approximately 10–15 nm, alternate mechanisms including grain boundary sliding, grain rotation and Coble creep have all been postulated to operate in conjunction with dislocation processes whereas at grain sizes of 5–10 nm, dislocation activity apparently ceases completely. There is no direct experimental evidence at present to substantiate these postulates; some of the computational methods utilized to arrive at these conclusions, such as molecular dynamics, operate in unrealistic stress–strain rate regimes that preclude time-dependent deformation processes. Experimental analogues employing the two-dimensional Bragg–Nye bubble raft models with nanocrystalline grains also reveal that when localized deformation is induced by recourse to indentation, a noticeable transition from strengthening to weakening with decreasing grain size occurs at a critical grain size of approximately 7 nm [42]. This transition is also accompanied by a change in mechanism from dislocation nucleation at grain boundaries to more pronounced grain boundary sliding and migration. It should be noted, however, that

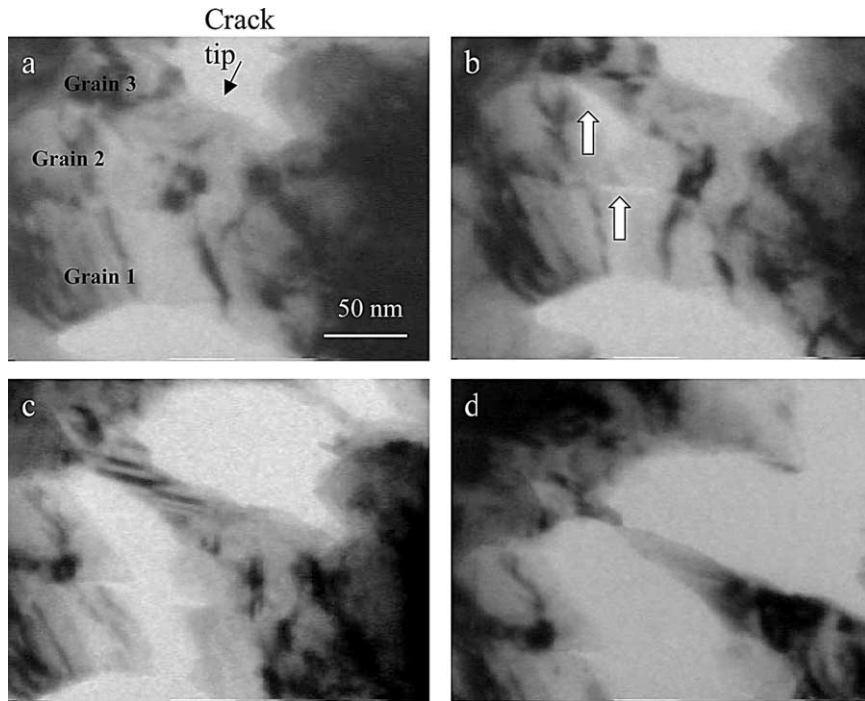


Fig. 11. A sequence of images extracted from a video-tape recording of the progression of deformation in an in situ straining experiment. In image (a), the crack tip and a ligament composed of three grains can be seen. This ligament has already undergone plastic deformation and the three grains are elongated. Further deformation results in grain boundary separation (b) and subsequent transgranular failure of grains 1 and 2 (c). The ligament left intact in (c) continues to deform plastically, developing parallel bands of alternate black-and-white contrast that could perhaps be a consequence of twinning. Eventually, the ligament necks down to a chisel point and ruptures (d). The digitized clip of this sequence of images may be viewed at <http://ninas.mit.edu/Submission/SupInfo/index2.html>.

experimental visualization tools such as the polycrystalline bubble raft model differ significantly from real nanocrystalline metals in terms of stress state effects, grain boundary structure and defect geometry.

Computational studies aimed at understanding deformation of nc-metals appear to focus only on the very early stages of deformation. How deformation evolves and ultimately leads to fracture in nc-metals remain unresolved issues. By comparing the deformation response of nc-Ni containing grain boundaries with various levels of disorder (i.e. equilibrium versus non-equilibrium) that simulate the as-deposited and annealed conditions, Hasnaoui et al. [43] concluded that grain boundary relaxation by a process such as annealing leads to a decrease in plasticity and increase in strength. They cite published experimental results on inert gas condensed nc-Cu [44] to support their con-

clusions, although the results of Ebrahimi et al. [12] on electrodeposited Cu (grain size 175–250 nm) suggest otherwise. It is possible that at these larger grain sizes (as opposed to 10–20 nm), the structure of the grain boundary is already close to equilibrium. Further experimental data are needed to verify the proposal of Hasnaoui et al. [43].

Results of uniaxial tensile tests reveal several unusual, hitherto unexplained, features specific to deformation of nc-metals with fcc structures. For instance, it is not fully understood as to why the tensile elongation to fracture of nanocrystalline metals is low relative to their conventional microcrystalline counterparts [13–15,18,40,41]. In the case of electrodeposited nc-Cu, two different conflicting reports [12,16] have been published: whereas Lu et al. [16] report tensile elongation values between 15 and 39% as a function of strain rate in the quasi-static strain rate regime ( $6 \times 10^{-5}$  to  $6 \times 10^{-2} \text{ s}^{-1}$ ),

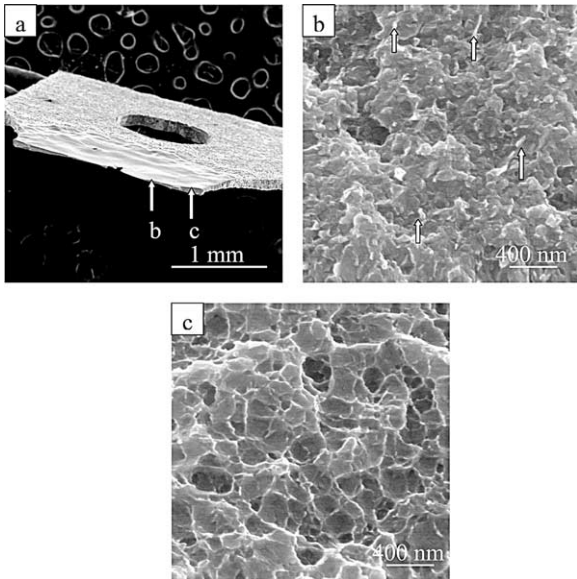


Fig. 12. A low magnification SEM image (a) of a fractured in situ tensile specimen provides a reference for the location of the high magnification images of the fracture surface shown in (b) and (c). The image in (b) representative of the thinner locations in the cross section, shows several highly deformed ligaments (a few are indicated with arrows), while in the thicker regions, dimpled rupture dominates (c), with the average dimple size being several grain diameters.

Ebrahimi et al. [12] report total elongation of  $< 2\%$  at a strain rate of  $1.8 \times 10^{-4} \text{ s}^{-1}$  in a similar pure metal processed similarly. The electrodeposited sheet thickness and average grain size reported

by Lu et al. [16] are 1.5 mm and 20–30 nm in comparison to 30  $\mu\text{m}$  and 175–250 nm reported by Ebrahimi et al. [12]. Surprisingly, however, the yield strength for Cu with a grain size of 20–30 nm is unusually low in [16] as compared to the values reported in the literature for a comparable grain size [14,15]. It is impressive that Lu et al. [16] were able to maintain such a fine grain size through the entire thickness of 1.5 mm by electrodeposition and it is perhaps the specimen thickness that accounts for the reported tensile elongation. In this context, Ebrahimi et al. [12] tested 100- $\mu\text{m}$  thick conventional cold-rolled copper along with their electrodeposited nc-Cu, and concluded that the low tensile elongation to fracture in these thin sheet specimens was a consequence of the early onset of plastic instability that localized deformation. The observation of *macroscopic* chisel-tip fracture in electrodeposited nc-Ni and nc-Cu [12,13] tensile tests with little tensile elongation to fracture supports the localized deformation hypothesis. Dalla Torre et al. [18] demonstrated that the shape of the stress–strain curve, tensile properties and fracture surface appearance of electrodeposited nc-Ni can all be affected by specimen size, with uniform deformation along the gauge section observed in small specimens (gauge length of 1.72 mm, thickness of 0.2 mm and width of 0.25 mm) but not in larger specimens (gauge length of 6 mm, thickness of 0.2 mm and width of 2.5 mm). They attribute the observed differences to microstruc-

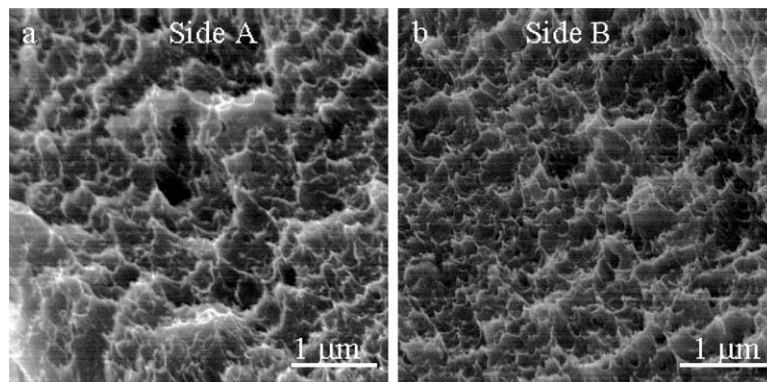


Fig. 13. A pair of SEM images (a,b) obtained from mating fracture surfaces of an in situ deformed tensile specimen of nc-Ni from source 2 [33,34]. The images were obtained from matching locations on the two surfaces and clearly confirm dimpled rupture on both surfaces.

tural inhomogeneity; they also conclude that intergranular fracture is the principal failure mode in the smaller specimens. This last observation contradicts the findings in the present study where dimpled rupture is evident.

In the early stages of permanent deformation, independent of the technique used to produce the nc-Ni or nc-Cu, a strong “work hardening” response is always observed [12–16,18] and in some cases, it appears to be stronger than in the microcrystalline counterparts [12,15]. Traditional explanations for high work hardening in fcc metals invoke mechanisms whereby the cross slip of dislocations is impeded, there is significant dislocation intersections and formation of locks. However, none of these processes has been experimentally or computationally demonstrated for nanocrystalline metals. Thus, it is not clear at present what mechanisms are responsible for this behavior. The results in the literature on the effect of strain rate on yield strength and tensile elongation appear controversial too. Whereas the results of Lu et al. [16] on electrodeposited nc-Cu and those generated in our laboratory on electrodeposited nc-Ni [40] illustrate an increase in both these properties with increasing strain rate in the quasi-static regime, this is not what is observed by Dalla Torre et al. [18] for electrodeposited nc-Ni. They [18] demonstrate a loss in tensile elongation with increasing strain rate with the ultimate tensile strength remaining virtually unchanged.

The ex situ deformation results from this study strongly point to the presence of dislocation activity during deformation while the in situ deformation in the TEM confirms this observation. It is important to understand, however, that in situ deformation of a thin foil specimen in the TEM is not representative of bulk behavior; recently it was computationally established [45] that dislocation processes can be more readily activated in a nc-metal that is two-grains thick than in the bulk. Nevertheless, when these observations are combined with those from a series of ex situ tests and observations of the fracture surfaces, together they provide a conclusive picture of the dominant deformation mode: dislocation-mediated plasticity.

The observations presented in this paper strongly indicate that the evolution of deformation

in electrodeposited nc-Ni and the eventual ductile fracture by dimpled rupture occur through the interplay of a variety of microstructural features. The mechanistic process envisioned from these observations is schematically illustrated in Fig. 14. In the early stages of deformation, dislocations are emitted from grain boundaries under the influence of an applied stress, when intragranular slip is coupled with unaccommodated grain boundary sliding to facilitate void formation at the grain boundaries [46]. Such voids do not necessarily form at every boundary. Triple junction voids and wedge cracks can also result from grain boundary sliding if resulting displacements at the boundary are not accommodated by diffusional or power law creep. These voids can grow and partially relieve the constraints on a grain or a small group of grains. Individual single-crystal ligaments so created deform extensively and finally experience chisel-point failure. These grain boundary and triple junction voids also act as sites for nucleation of the dimples which are significantly larger than the individual grains and the rim of these dimples on the fracture surface do not necessarily coincide with grain boundaries. Thus, at a local level, the nc-Ni demonstrates considerable plasticity. Its deformation and fracture processes are closely related to the coupling of dislocation-mediated plasticity and formation and growth of voids. It is well known that nanovoids filled with hydrogen (hydrogen bubbles) are often present in electrodeposited metals and these can also serve as nucleation sites for the dimples observed on the fracture surface without the need to nucleate voids during deformation [47]; the relative significance of hydrogen-induced nanovoid formation, however, would be strongly influenced by the specific processing conditions.

Lastly, the possibility that twinning could be an active deformation mode in a high-stacking fault energy metal like Ni deserves some discussion. The observations in Fig. 11 (and the associated video clip in the website for the supplementary information provided here) of parallel alternate bands of black and white contrast appears to be ascribable to deformation twinning, although diffraction patterns to confirm twinning were not obtained. Deformation twinning in face centered

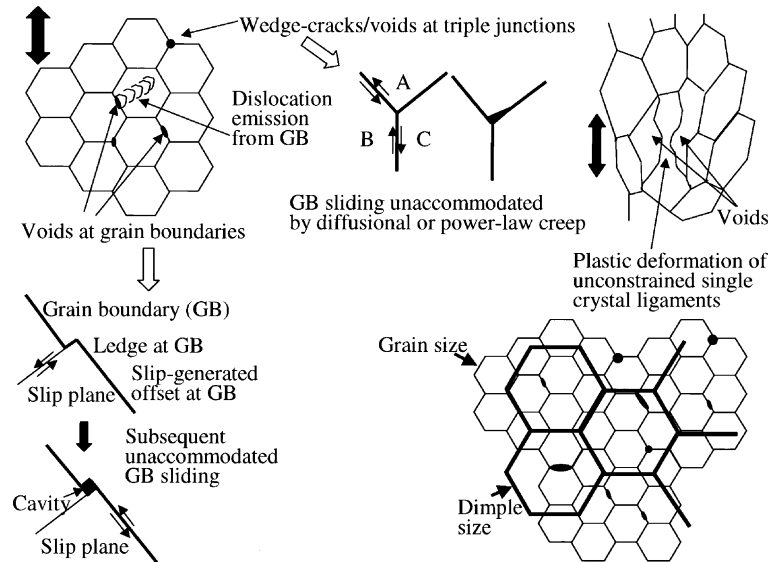


Fig. 14. A schematic illustration depicting how deformation evolves in the nanocrystalline nickel examined in this study. Dislocation motion, void formation/growth at grain boundaries and triple junctions, the formation of partially unconstrained ligaments that deform plastically, and the interaction of these various features to produce the eventual fracture morphology are all synthesized in this figure.

cubic metals is possible and has been observed in a variety of fcc metals and solid solution alloys [48]. Embury et al. [49] have provided the criteria for the onset of twinning in fcc metals which require two conditions to be met simultaneously: (i) a change in the dominant slip system needs to occur, and (ii) a critical stress level needs to be reached. For deformation twinning in nickel to occur, a resolved shear stress of the order of 300 MPa is required [48]. These stress levels are often easily reached in these nanocrystalline metals and thus it is not inconceivable that twinning could occur in the single crystal ligaments when the criteria identified in [49] are met.

## 6. Concluding remarks

A comprehensive experimental investigation has been performed to document the mechanisms of deformation and damage evolution in in situ and ex situ deformed nanocrystalline Ni, by recourse to state-of-the-art electron microscopy tools. The material chosen for this investigation was electrodeposited Ni with an average grain size of

approximately 30 nm and a narrow grain size distribution. The as-deposited material was examined in the electron microscope, at Angstrom-level resolution, to establish that the grain interiors were clean and devoid of dislocations, and that the grain boundaries did not contain any amorphous layers or second-phase particles, or nano-scale voids. Cross-sectional TEM observations revealed that the nanocrystalline grains exhibited a columnar grain structure that also comprised growth twins.

Observations of ex situ deformed specimens of the nanocrystalline Ni, following compression, rolling and nanoindentation, indicated that crystallinity was maintained right up to the grain boundary, while isolated dislocations, evidence of sporadic dislocation networks and some dislocation debris were seen within grains. In all three cases of ex situ deformation, the density of dislocations left in the specimens could not account for the high levels of imposed plastic strains.

In situ tensile tests were conducted in a transmission electron microscope and, from these experiments, sequential still images as well as video clips of deformation and damage evolution were extracted. Some of these video images are available

for observation in the supplementary website accompanying this publication: <http://ninas.mit.edu/Submission/SupInfo/index2.html>. These in situ experiments provide very compelling and direct evidence for copious dislocation activity in the nanocrystalline Ni. Deformation is instigated by the emission of dislocations at grain boundaries whereupon voids and/or wedge cracks form along grain boundaries and triple junctions as a consequence of transgranular slip and unaccommodated grain boundary sliding. The growth of voids at separated grain boundaries results in partial relaxation of constraint, and continued deformation causes the monocrystalline ligaments separating these voids to undergo significant plastic flow that culminates in chisel-point failure. Thus, dislocation mediated-plasticity in concert with the nucleation and growth of voids provides appreciable local plasticity in the deformation of the nanocrystalline metal. Ex situ and in situ deformed specimens exhibit similar fracture surface features that primarily reveal the occurrence of dimpled rupture. The dimples nucleated by the voids grow to some six to ten times of the average grain size. The possible presence of nanovoids filled with hydrogen in the electrodeposited Ni could further contribute to the nucleation of dimples seen on the fracture surfaces. The in situ experiments also reveal the formation of twins. Such twinning in the present face-centered cubic metal could be envisioned as a possibility since the local resolved shear stress can easily exceed a critical value, approximately 300 MPa, in the present nano-Ni.

The foregoing observations are synthesized in such a manner that a mechanistic basis for rationalizing the experimental results of mechanical response in nanocrystalline metals is formulated.

### Acknowledgements

This work was supported by the Defense University Research Initiative on NanoTechnology (DURINT) on “Damage- and Failure-Resistant Nanostructured and Interfacial Materials” which is funded at the Massachusetts Institute of Technology (MIT) by the Office of Naval Research under grant N00014-01-1-0808. The authors also

acknowledge additional support from the Division of Materials Sciences and Engineering, Office of Basic Energy Sciences, US Department of Energy under contract DE-AC05-00OR22725 with UT-Battelle, LLC. Thanks are due to K. J. Van Vliet for assistance with nanoindentation and to T.G. Nieh of Lawrence Livermore National Laboratory and Integran Technologies, Inc. of Toronto, Canada for providing the electrodeposited nickel sheets.

### References

- [1] Gleiter H. *Prog Mater Sci* 1989;33:223–315.
- [2] Suryanarayana C. *Inter Mater Rev* 1995;40:41.
- [3] Jeong DH, Gonzalez F, Palumbo G, Aust KT, Erb U. *Scripta Mater* 2001;44:493.
- [4] Schuh C, Nieh TG, Yamasaki T. *Scripta Mater* 2002;46:735.
- [5] Lu L, Sui ML, Lu K. *Science* 2000;287:1463.
- [6] McFadden SX, Mishra RS, Valiev RZ, Zhilyaev AP, Mukherjee AK. *Nature* 1999;398:684.
- [7] Sanders PG, Fougere GE, Thompson LJ, Eastman JA, Weertman JR. *Nanost Mater* 1997;8:243.
- [8] Tellkamp VL, Melmed A, Lavernia EJ. *Metall Mater Trans* 2001;32A:2335.
- [9] Valiev RZ, Islamgaliev RK, Alexandrov IV. *Prog Mater Sci* 2000;45:103.
- [10] Erb U. *Nanost Mater* 1995;6:533.
- [11] El-Sharik AM, Erb U, Palumbo G, Aust KT. *Scripta Metall Mater* 1992;27:1185.
- [12] Ebrahimi F, Zhai Q, Kong D. *Scripta Mater* 1998;39:315.
- [13] Ebrahimi F, Bourne GR, Kelly MS, Matthews TE. *Nanost Mater* 1999;11:343.
- [14] Legros M, Elliott BR, Rittner MN, Weertman JR, Hemkar KJ. *Philos Mag A* 2000;80:1017–26.
- [15] Sanders PG, Eastman JA, Weertman JR. *Acta Mater* 1997;45:4019.
- [16] Lu L, Li SX, Lu K. *Scripta Mater* 2001;45:1163.
- [17] Nieman GW, Weertman JR, Siegel RW. *J Mater Res* 1991;6:1012.
- [18] Dalla Torre F, Van Swygenhoven H, Victoria M, *Acta Mater*, in press.
- [19] Chokshi AH, Rosen A, Karch J, Gleiter H. *Scripta Metall* 1989;23:1679.
- [20] Masumura RA, Hazzledine PM, Pande CS. *Acta Mater* 1998;46:4527.
- [21] Schiotz J, Di Tolla FD, Jacobsen KW. *Nature* 1998;391:561.
- [22] Schiotz J, Vegge T, Di Tolla FD, Jacobsen KW. *Phs Rev B* 1999;60(1):1197.
- [23] Van Swygenhoven H, Spaczer M, Caro A. *Acta Mater* 1999;47:3117.

- [24] Van Swygenhoven H, Spaczer M, Caro A, Farkas D. *Phs Rev B* 1999;60:22.
- [25] Van Swygenhoven H, Derlet PM. *Phs Rev B* 2001;64:224105.
- [26] Derlet PM, Van Swygenhoven H. *Philos Mag A* 2002;82:1.
- [27] Yamakov V, Wolf D, Salazar M, Phillpot SR, Gleiter H. *Acta Mater* 2001;49:2713.
- [28] Van Swygenhoven H, Derlet PM, Hasnaoui A. *Phys Rev, B* 2002;66:024101.
- [29] Milligan WW, Hackney SA, Ke M, Aifantis EC. *Nanost Mater* 1993;2:267.
- [30] Youngdahl CJ, Weertman JR, Hugo RC, Kung HH. *Scripta Mater* 2001;44:1475.
- [31] McFadden SX, Sergueeva AV, Kruml T, Martin J-L, Mukherjee AK. *MRS Proceedings* 2001;634:B1.
- [32] Veyssièrè P, Saada G. In: Nabarro FRN, Duesbery MS, editors. *Dislocations in solids*. Elsevier Science; 1996. p. 255–441 Chapter 53.
- [33] El-Sherik AM, Erb U. *Jour Mater Sci* 1995;30:5743.
- [34] Erb U, El-Sherik AM. US patent No. 5,353,266 (1994).
- [35] Siegel RW, Thomas GJ. *Ultramicroscopy* 1992;40:376.
- [36] Thomas GJ, Siegel RW, Eastman JA. *Scripta Metall Mater* 1990;24:201.
- [37] Van Swygenhoven H, Farkas D, Caro A. *Phys Rev B* 2000;62:831.
- [38] Wunderlich W, Ishida Y, Maurer R. *Scripta Metall Mater* 1990;24:403.
- [39] Keblinski P, Wolf D, Phillpot SR, Gleiter H. *Scripta Mater* 1999;41:631.
- [40] Dao M, Kwon YN, Chollacoop N, Suresh S. 2002, unpublished research.
- [41] Mukai T, Suresh S, Kita K, Sasaki H, Kobayashi N. 2002, unpublished research.
- [42] Van Vliet KJ, Tsikada S, Suresh S. 2002, unpublished research.
- [43] Hasnaoui A, Van Swygenhoven H, Derlet PM. *Acta Mater*, 2002, in press.
- [44] Weerman JR, Sanders PG. *Solid State Phenom* 1994;35-36:249.
- [45] Derlet PM, Van Swygenhoven H. *Philos Mag A* 2002;82:1.
- [46] Courtney TH. In: *Mechanical behavior of materials*. McGraw-Hill Series in Materials Science and Engineering. New York: McGraw-Hill, Inc.; 1990. p. 517–21.
- [47] Nakahara S. *Acta Metall* 1988;36:1669.
- [48] Honeycombe RWK. *The plastic deformation of metals*. New York: St. Martin's Press; 1968. p. 210–7.
- [49] Embury JD, Szczerba MS, Basinski ZS, Yoo MH, Wuttig M, editors. *Twinning in advanced materials*. Warrendale, PA: The Minerals, Metals and Materials Society; 1994. p. 331–6.